Kapitza conductance of symmetric tilt grain boundaries in graphene

Ajing Cao and Jianmin Qu

Citation: J. Appl. Phys. **111**, 053529 (2012); doi: 10.1063/1.3692078
View online: http://dx.doi.org/10.1063/1.3692078
View Table of Contents: http://jap.aip.org/resource/1/JAPIAU/v111/i5
Published by the American Institute of Physics.

Kapitza conductance of symmetric tilt grain boundaries in graphene

Ajing Cao and Jianmin Qu[a)]
Department of Civil and Environmental Engineering, Department of Mechanical Engineering, Northwestern University, Evanston, Illinois 60208, USA

(Received 9 November 2011; accepted 8 February 2012; published online 9 March 2012)

Non-equilibrium molecular dynamics simulations were employed to study the Kapitza conductance of symmetric tilt grain boundaries in the monolayer graphene sheet. Both armchair and zig-zag oriented bicrystal graphene were investigated. The Kapitza conductance of the interface shows length dependence up to 300 nm, which arises from the fact that long-wavelength phonons allowed in large-size graphene are able to transmit through the interface contributing to the Kapitza conductance. The Kapitza conductance exhibits monotonic increase with temperature, opposite to the trend of thermal conductivity of bulk graphene above room temperature. We found that the Kapitza conductance is inversely proportional to the number of dislocations per length of grain boundaries. The facts that the phonon density of states (DOS) shows no difference between the two crystals separated by the grain boundary and the vibrational DOS of grain boundary region atoms deviates from that of bulk atoms reveal that the interfacial thermal resistance arises from the structure defects, causing additional phonon scattering for the mismatched phonon spectrum of defects. The predicted length-independent Kapitza conductance ranges from 19 to 47 GW/Km^2, which is larger than that of any other interfaces reported in the literature. Finally, theoretical analysis was carried out to explain why the thermal resistance scales with the number of defects per unit length. © *2012 American Institute of Physics*. [http://dx.doi.org/10.1063/1.3692078]

I. INTRODUCTION

Monolayer graphene, a two-dimensional (2D) material, owing to its unique thermal,[1–3] optical,[4] electrical,[5,6] and mechanical properties,[7] has opened new avenues in physics exploration and future technology. Its potential applications include high-frequency electronic devices,[8,9] single molecule gas detection,[10] transparent conducting electrodes,[10] composites,[11] and energy storage devices,[12] such as super-capacitors and lithium ion batteries,[10] etc. With the broad physical intriguing properties and potentials to be able to change conventional technologies in various fields, there is no doubt that graphene has become a promising candidate for new materials for future electronic and composite material industry.

Recently, graphene together with carbon nanotubes (CNTs) has been proposed as thermal interface materials to dissipate heat along the pathway from the heat source (e.g., Si chip) to the heat spreader in NEMS devices.[13] It is therefore crucial to understand the fundamental thermal transport physics at the interfaces in this unique material. More recently, a chemical vapor deposition (CVD) technique has been developed to grow graphene on metal foils, such as nickel[14,15] and copper.[16,17] A natural outcome of this technique is that the grain boundaries are ubiquitous in large-area graphene sheets, because each grain in the metallic foil serves as a nucleation site for individual grains of graphene. Thus the application of CVD-grown polycrystalline graphene in future nanotechnology demands a full understanding of the structure of grain boundaries and the effect of grain boundaries on its physical properties. Graphene edges and point defects, such as vacancies and stone-walls have been extensively investigated over the past few years.[18] It is anticipated that properties of 2D materials can be strongly affected by structural irregularities. However, the role of grain boundaries on the thermal conductivity of polycrystalline graphene has not been well-documented yet. In this paper, we address the role of grain boundary (GB) on the thermal properties of bicrystal graphene consisting of tilt grain boundaries by employing non-equilibrium molecular dynamics (MD) simulations. In this study, we limit our focus to symmetric tilt grain boundaries since asymmetric configurations tend to result in diverging elastic energies.[19]

As this paper was being prepared, a publication appeared[20] which studied thermal transport behavior in zig-zag-orientated graphene twin boundaries using MD simulations. In that paper, a reverse non-equilibrium MD (RNEMD) approach was adopted and the heat flux was applied by exchanging kinetic energy between two groups of atoms in different regions of the simulation box every N ($N > 0$ and is an integer) steps. The essential physical idea is the same as the present study: both approaches impose a temperature gradient on the system and measure the response as the resulting heat flux. They found the boundary conductance to be in the range 1.5×10^{10} to 4.5×10^{10} W/Km.[2] However, the mechanistic explanations for the interfacial thermal resistance due to the presence of grain boundaries were not provided. In the present paper, our major results are the following: (1) We obtained the length independent Kapitza conductance by simulating large enough systems with lengths from 50 nm to 400 nm. (2) We established the structure-thermal property relationship by studying a variety of bicrystal configurations including both zig-zag and armchair

[a)]Electronic mail: j-qu@northwestern.edu.

oriented graphene. (3) Our detailed vibrational density of state analysis reveals the origin of the interfacial thermal resistance. (4) The temperature dependence of Kapitza conductance is also reported.

The paper is arranged as follows: Following this introduction, which presents the background and outlines the motivations, Sec. II describes the grain boundary structures and the simulation methodology we used in the simulations. In Sec. III, the simulation results along with analysis of phonon density of state (DOS) are presented. To explain the results observed, a theoretical analysis based on phonon the Boltzmann transport equation and the kinetic law of thermal conductivity is carried out. Finally, the main findings are summarized together with concluding remarks in Sec. IV.

II. GRAIN BOUNDARY STRUCTURES AND SIMULATION METHODOLOGY

A. Grain boundary structures

The model system of graphene consists of a square cell geometry with grain boundary in the middle of the length direction (X axis). A schematic of the simulation models mimicking a suspended graphene sheet placed on top of a trench adopted in the present work is shown in Fig. 1.

The length of graphene in this study varies from 20 to 400 nm. The structures of tilt grain boundaries in zig-zag and armchair-oriented graphene are shown in Fig. 2 for various tilt angles. The grain boundaries consist of repeating five- and seven-membered ring pairs (5–7 pairs) that are separated by several hexagonal rings. From the picture, one can observe that in the zig-zag-oriented graphene, the number of hexagonal rings separating the 5-7 defects decreases as the misorientation angle increases, with the limit occurring at 21.7° in which only a single hexagonal ring separates the periodic 5-7 defects. Likewise, in the armchair-oriented graphene, 28.7° is the highest defect density as 5-7 ring pairs are the only components in the grain boundaries. Therefore, the trend is clear in the two cases: bicrystals with larger grain boundary tilt angles contain higher defect densities. The repeating defect pairs can also be thought of as an array of edge dislocations with horizontal Burgers vectors where the five-membered rings represent the extra plane of atoms. To be specific, the defects can be classified in two categories. The two types of dislocations, namely (1,0) dislocation, and (1,0) + (0,1) dislocation pair are the building blocks in the two bicrystal graphene, which has been studied by other groups.[21] The configurations of the two types of dislocations are shown in Fig. 3. These structural irregularities are thought to be the origin of interfacial thermal resistance and deserve detailed analysis as will be shown in the next section. We believe that dislocation density plays a vital role in determining the thermal conductivity of bicrystal graphene as we will present in the next section.

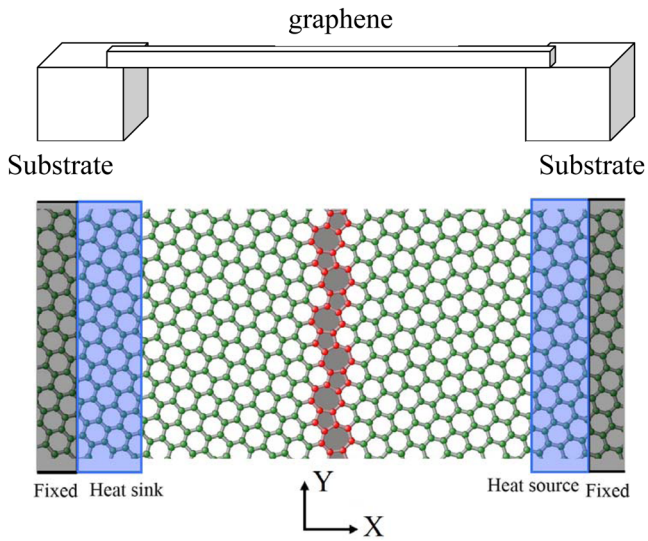

FIG. 1. (Color online) The non-equilibrium MD simulation model employed in our study. (a) The top panel is the experimental setup with graphene sitting over a trench as shown in Ref. 15. (b) Top view of the model. The bicrystal grain boundary is located at the middle along the length direction. Defected rings are in the gray shadow. Two regions at the two ends are fixed (black boxes in color version and dark in the black and white version). The heat source is placed at a region next the right-hand end (blue boxes in color version and light in the black and white version) and heat sink is at the simulation cell on the left-hand end. Note that PBC is not used in the length direction (X) while PBC is used in the width direction (Y) of graphene.

B. Simulation methodology

The essential idea of non-equilibrium MD method is to impose a temperature gradient by applying a heat flux along the graphene length direction. Thermal conductivity of graphene can then be obtained from the heat flux and the temperature gradient along the length direction using the well-known Fourier's law,

$$\kappa = -\frac{J_x}{\partial T/\partial x}, \tag{1}$$

where J_x is the heat flux, and $\partial T/\partial x$ is the spatial temperature gradient.

In our calculations, the atoms at the two ends (2 nm of length) were chosen to be fixed without movement. The heat source consisting of 2 nm sitting next to the fixed region was placed at right-hand end of the simulation cell and the heat sink of same size was chosen to be next to the left-hand fixed end of the graphene (see Fig. 1(b)). This way, the model was intended to simulate the situation that a suspended graphene sitting over a trench, as the setup in experiment.[22] To avoid a third interface and asymmetric temperature profile across the boundary as seen in Ref. 20, period boundary condition (PBC) was not used along the graphene length direction while PBC was applied in the width direction. The energy transport algorithm proposed by Jund and Jullien[23] was employed. In this manner, once steady state (i.e., the temperature profile along the length direction does not change with time) was reached, a constant temperature gradient from the heat source to heat sink was established. After reaching steady state, time average of temperature over 100 ps was used to perform ensemble sampling. Such statistically averaged temperature profile was then used to compute the temperature gradient using the standard linear regression method. Standard deviation associated with the linear

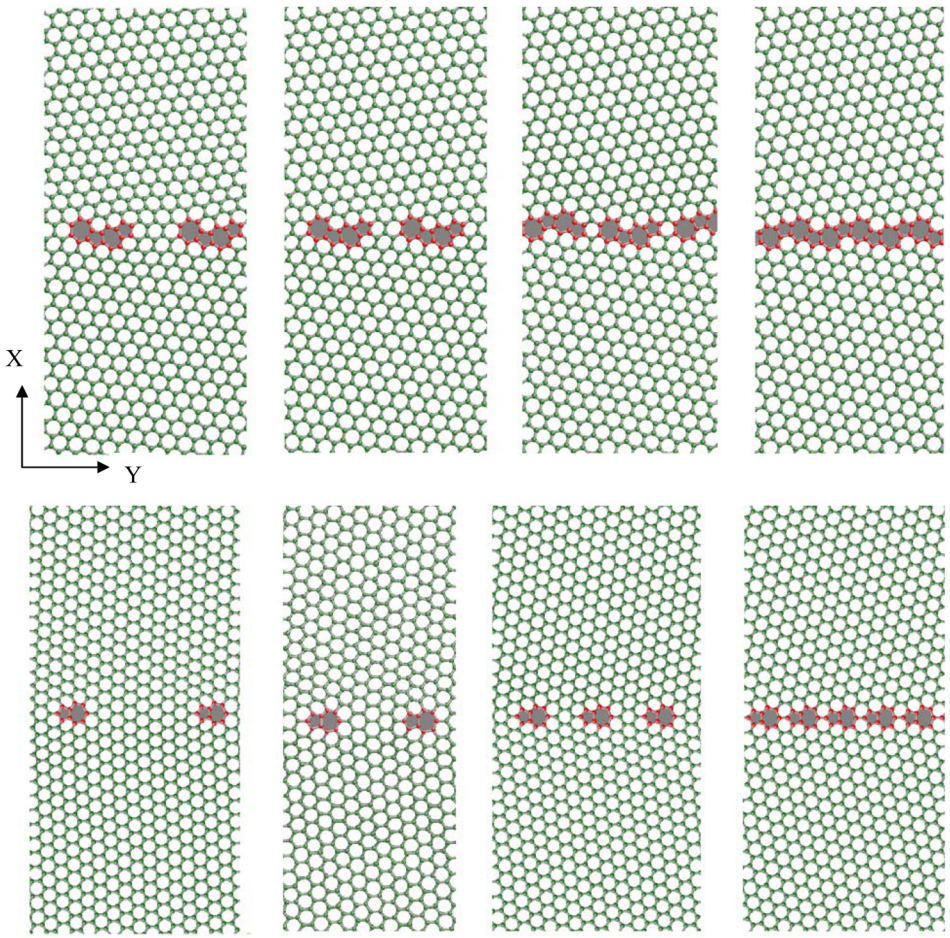

FIG. 2. (Color online) The structure of tilt grain boundaries with misorientation angles of (a) armchair-oriented bicrystals (15.18°, 17.9°, 21.4°, 28.7°) and (b) zig-zag-oriented bicrystals (5.5°, 9.8°, 13.2°, 21.7°). The corresponding dislocation densities of each are shown in Tables I and II.

regression of the temperature profile was reported in our results by error bars.

All MD simulations were simulated with the LAMMPS software package.[24] A time step of 0.5 fs was used. The optimized Tersoff potential[25] has been demonstrated to have the best agreement of dispersion curves prediction of graphene and experimental data of in-plane graphite.[26,27] Therefore, the optimized potential was used in the present study.

Because of the different periodicity along the width direction for different bicrystal graphene, the same heat flux $J_x = Q/At$ and same length L were used for fair comparison. In addition, because of the PBC used along the width direction of the graphene, we are effectively simulating a graphene sheet of infinite width. We have found that doubling the width introduces no appreciable difference in the results once the width is larger than 5 nm. In addition, varying the length of the temperature-controlled region from 2 nm to 10 nm does not change the results. The graphene cross-section area is considered to be wh, where w and h are the width and thickness of the graphene, respectively. Here $h = 0.34$ nm.

III. SIMULATION RESULTS

A. Temperature profile

A typical temperature profile of graphene consists of a grain boundary is shown in Fig. 4(a). Clearly, there is a sharp temperature discontinuity at the interface. In contrast, the temperature in the pristine graphene case is continuous all along the length direction, as shown in Fig. 4(b).

According to the Fourier law, the interfacial thermal conductance also known as the Kapitza conductance[28] can be defined by

TABLE I. The dislocation density per unit length and G_k for armchair-oriented graphene bicrystals of various tilt angles.

GB misorientation angle	Dislocation density (nm^{-1})	G_k (GW/Km^2)
15.18°	1.260	26.75
17.9°	1.484	24.96
21.4°	1.804	24.32
28.7°	2.293	18.72

TABLE II. The dislocation density per unit length and G_k for zig-zag-oriented graphene bicrystals of various tilt angles.

GB misorientation angle	Dislocation density (nm^{-1})	G_k (GW/Km^2)
5.5°	0.398	46.81
9.8°	0.679	43.04
13.2°	0.948	35.66
21.7°	1.563	26.75

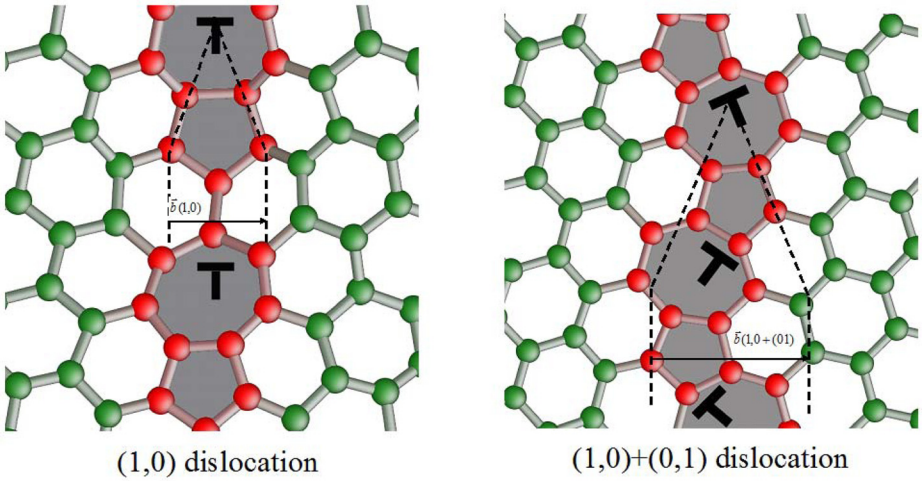

FIG. 3. (Color online) The detailed atomic structures of (1,0) dislocation, and a (1,0) + (0,1) dislocation pair, respectively. The dashed lines point out the introduced semi-infinite strips of graphene originating at the dislocation core. Defect atoms are in red color (dark in the black and white version) while bulk atoms are in green color (light in the black and white version). Non-six-membered rings are in shadow. Atomic structures of the $\theta = 21.8°$ zig-zag-oriented bicrystal (left) and the $\theta = 32.2°$ armchair oriented bicrystal (right) symmetric large-angle grain boundaries, respectively.

$$G_k = \frac{J_x}{\Delta T}, \tag{2}$$

where J_x and ΔT are the heat flux across the interface and temperature drop at the interface, respectively.

In this study, the temperature drop ΔT at the interface was done as follows: (1) a linear regressions of the two temperature profiles separated by the interface were done independently. (2) The temperature difference between the two intersections of the two linear regression lines with the interface was considered as the temperature drop at the interface. Once we have the temperature drop at the interface, we can compute the interfacial thermal conductance G_k based on Eq. (2) right away.

B. Length effect on G_k

Shown in Fig. 5 *are our results for the Kapitaza conductance* G_k of both armchair and zig-zag-oriented bicrystal graphene along with that of pristine graphene at $T = 300$ K. It is seen that both the zig-zag and armchair-oriented graphene show a similar trend, i.e., the Kapitza conductance increases with increasing conducting length. Specifically, it seems that Kapitza conductance increases linearly with length and saturates at between 200 and 300 nm, which is the effective ballistic length. The results are in good agreement with the situation that graphene contacted with Si block in our recent independent study,[13] in which we found beyond 200–300 nm, the Kaptiza conductance of graphene/Si interface does not vary with conducting length. The consistent results indicate that chemically bonded interfaces have a strong influence in diffusing phonons with wavelengths shorter than the effective ballistic length in graphene, which is 200–300 nm. Although the variation of G_k is smaller compared to the thermal conductivity change of graphene on the length, the origin for such variation should be universal, i.e., the long-wavelength phonons only present in long graphene are able to transmit the interface and therefore enhance the contribution to the overall interfacial thermal conductance and thus result in larger interfacial thermal conductance.

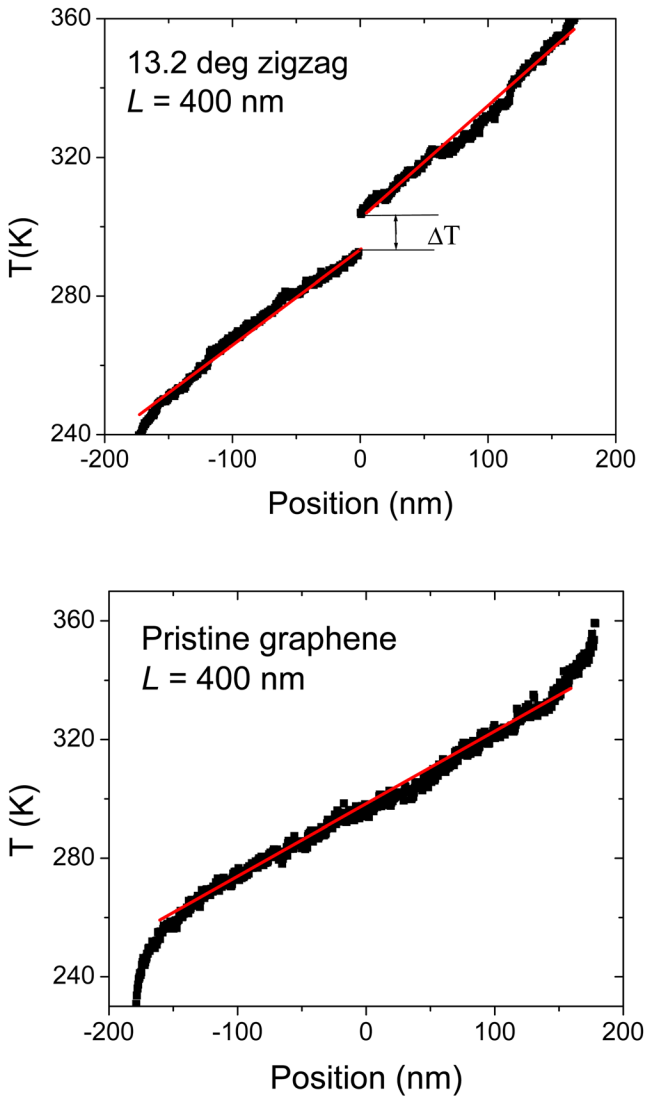

FIG. 4. (Color online) One typical temperature profile of a 13.2° zig-zag-oriented bicrystal graphene and a pristine zig-zag graphene, showing the temperature drop at the grain boundary interface and nice linear temperature profile in pristine graphene without interfaces.

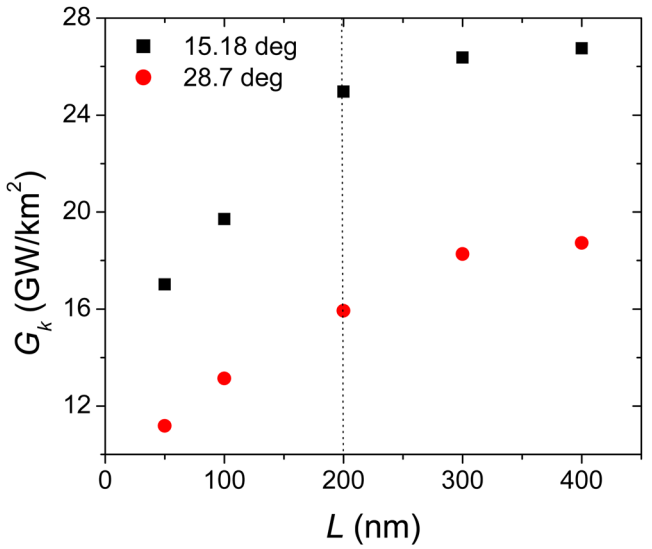

FIG. 5. (Color online) G_k as a function of graphene thermal conducting length for both 15.18° and 28.7° armchair-oriented bicrystal. Both show G_k scales with length and saturate about 200-300 nm, which is about the phonon effective ballistic length of graphene.

A similar trend has been found in Si-Ge (Ref. 29) and silicon grain boundaries[30] and graphene/Si interface.[31]

Another intriguing result of our study is that the dislocation type plays a significant role, as shown in Fig. 6(b). The reason that grain boundaries consists of (1,0) type dislocations has higher Kapitza conductance is probably because the heat flow is perpendicular to the interface, giving the incidental phonon less chance to revert back and a greater chance to transmit through the interface while heat flow is inclined to the grain boundaries zig-zag paths composed of (1,0) + (0,1) dislocation pairs, which presumably involves more phonon scattering at the interfaces.

C. G_k as a function of GB misorientation angle and dislocation density

The results of G_k as a function of GB misorientation angle for all studied cases are summarized in Fig. 6(a). We realize that dislocation density is a more fundamental parameter than GB misorientation angle to characterize the properties of bicrystal graphene. Here, we plot the results of Kaptiza conductance as a function of dislocation density in Fig. 6(b). Clearly, a linear relationship can be observed for both (1,0) dislocation and (1,0) + (0,1) dislocation pair type of grain boundaries. The length independent Kaptiza conductance we obtained for all bicrystals studied is in the range of 19–47 GW/Km,[2] which is in good agreement with recent report but with different simulation approach.[20] It is worth noting that these values are one order higher than the value reported in other interfaces such as Si-Si (001) Σ29 grain boundaries,[30] Si-Ge interfaces,[29] and CNT/Si interfaces.[32] The extremely high value of the bulk thermal conductivity and relatively high interfacial thermal conductance of graphene suggests that graphene is beneficial for electronic applications and establishes graphene as an excellent material for thermal management.

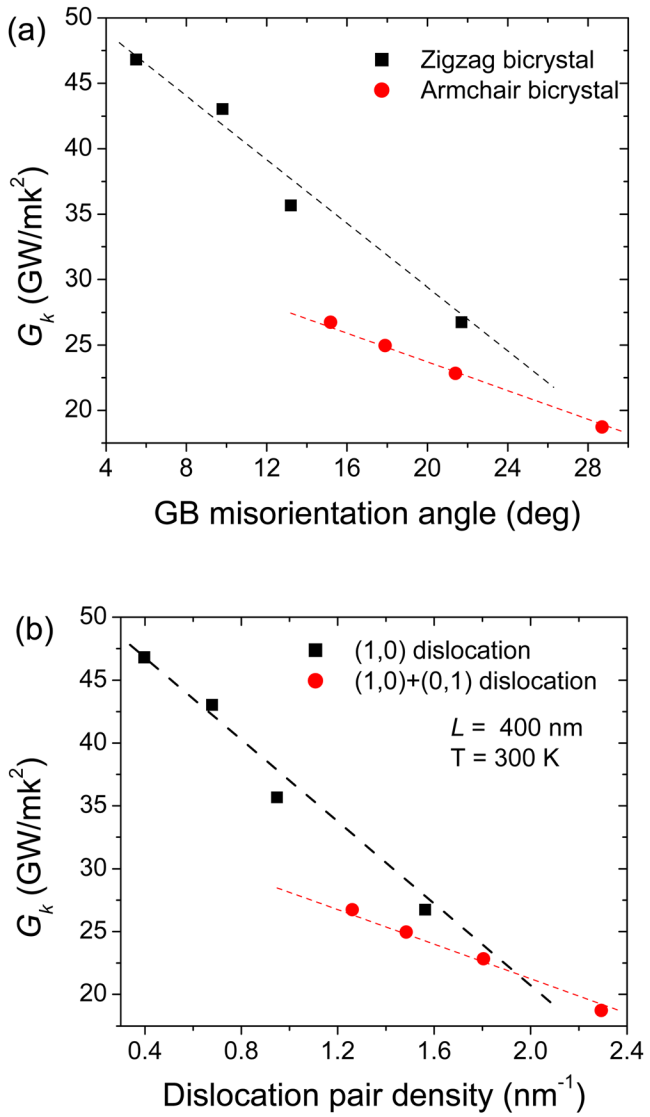

FIG. 6. (Color online) (a) G_k as a function of GB misorientation angle for both armchair and zig-zag oriented bicrystal graphene. (b) G_k as a function of dislocation density. Both show clear linear decrease of Kapitza conductance with increasing dislocation density. The dashed lines are guides for the eye.

D. The effective thermal conductivity

In terms of the effective thermal conductivity, we simply use

$$\kappa_{eff} = -\frac{J_x}{\Delta T/\Delta x}, \tag{3}$$

where ΔT and Δx being temperature difference at the heat source and heat sink and conducting length, respectively. The approximation is made by assuming the temperature discontinuity is negligibly small and a linear temperature profile is still valid for the Fourier law to be able to apply. This is in practice an important value because the entire temperature profile in most experiments is not available and the temperature difference at the two heat reservoirs is the only information one can get with technique like infrared microscopy.[33] Therefore, the effective thermal conductivity is a fairly good index dictating the overall thermal transport capability of a piece of graphene as a whole and the exact microstructure

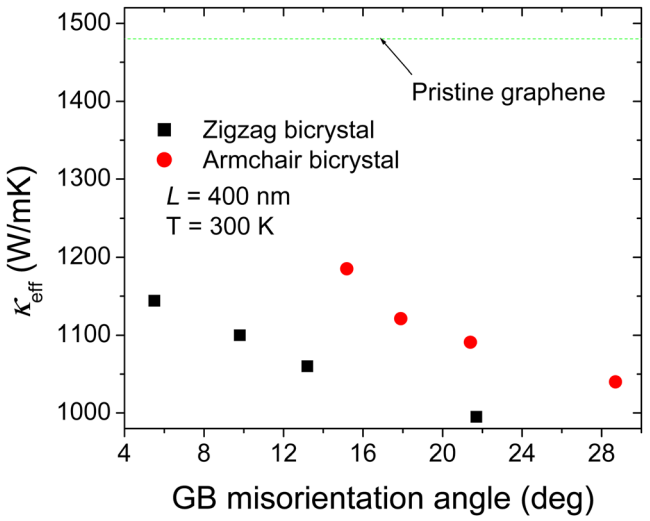

FIG. 7. (Color online) The effective thermal conductivity as a function of GB misorientation angle for both armchair and zig-zag bicrystal graphene compared with that of pristine graphene of the same length $L = 400$ nm at $T = 300$ K. Note because of the temperature discontinuities in bicrystal graphene, the "effective" thermal conductivity is calculated based on the temperature difference at the heat source and heat sink.

details are not necessarily known. The results of effective thermal conductivity of bicrystal as a whole are shown in Fig. 7, which shows monotonic decrease with increasing GB misorientation angle as well.

E. Temperature dependence on G_k and κ

The calculated temperature dependence of the Kapitza conductance and the thermal conductivity is shown in Figs. 8(a) and 8(b). Surprisingly, the Kapitza conductance has the opposite trend of the thermal conductivity. That is, the Kapitza conductance monotonically increases with temperature while the thermal conductivity shows a $\kappa \sim 1/T$ relationship at elevated temperature regime. The trend of graphene's thermal conductivity is identical to that of carbon nanotubes[34,35] and agrees reasonably well with another theoretical study of graphene.[36]

Thermal resistance R, which is the inverse of thermal conductivity κ, in graphene for example, mainly comes from the phonon-phonon umklapp scattering. Such scattering is enhanced at higher temperatures, resulting in higher thermal resistance in bulk graphene. The grain boundary interfacial thermal resistance, on the other hand, comes primarily from two processes, namely, phonon scattering by structure defects (lattice mismatch) at the interface, and the phonon spectra

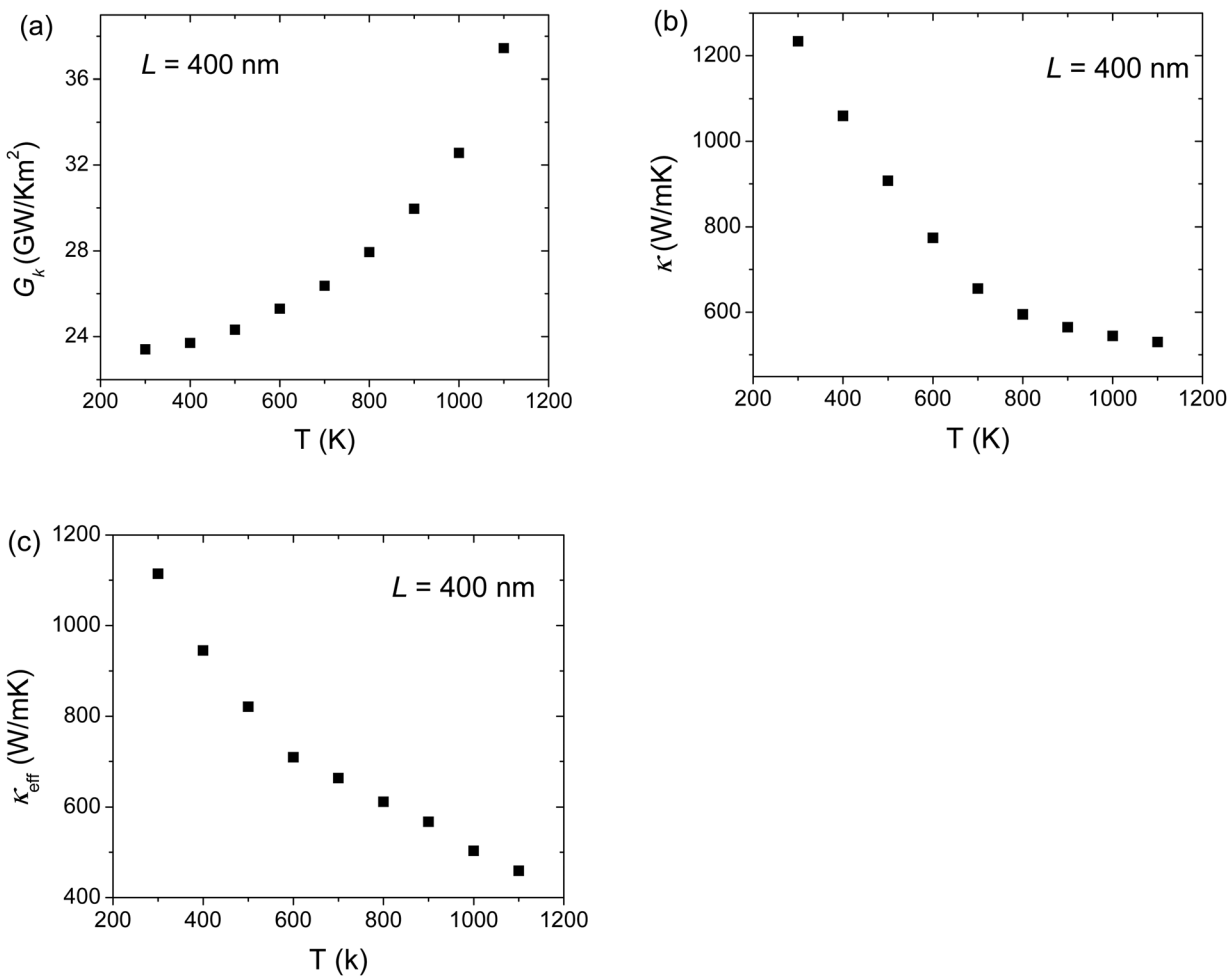

FIG. 8. (a) Temperature dependence of G_k of 21.7° zig-zag-oriented bicrystal graphene, showing the opposite trend of temperature dependence of κ above room temperature in (b). (c) The effective thermal conductivity of the whole system including the interface as a function of temperature.

mismatch between interfacial atoms and bulk atoms, as will be shown in the next section. As temperature increases, the phonon spectrum mismatch is expected to be reduced and thus yields lower interfacial thermal resistance. It is important to note that the effective thermal conductivity as a whole of the system is reduced at higher temperatures, as shown in Fig. 8(c), as a consequence of temperature sensitivity of thermal conductivity wining over that of the Kapitza conductance. In other words, the resistance due to umklapp scattering process plays a more important role, comparing with that of phonon-defect scattering at grain boundaries.

F. Phonon density of states

Next we proceed to gain some fundamental physical understandings on why such interfacial thermal resistance exists. Generally speaking, there are two plausible scenarios: (1) phonon spectral mismatch for the crystals separated by the grain boundaries similar to dissimilar materials do; (2) because grain boundaries in this work can be deemed as collective group of five- and seven ring dislocations, the structure defects themselves are barriers for phonon to pass through and therefore create temperature inhomogeneities and are responsible for the interfacial thermal resistance. The two mechanisms are quite different in the sense that the first mechanism is primarily dominated by the thermal properties of the two crystals rather than the local behavior of atoms located at grain boundary regions. As a consequence, strategies to reduce the interfacial thermal resistance are quite different: corresponding to the first one is to reduce the phonon spectral mismatch of the two crystals while the latter one is to decrease defect density as much as possible.

To gain insights on the origin of the interfacial thermal resistance at the grain boundaries, we have examined the phonon vibrational DOS for the two separated crystals. An additional simulation was conducted for the 15.18° armchair bicrystal graphene, which consists of a 3 nm × 100 nm simulation cell with periodic boundary conditions in both in-plane directions. The atomic velocity was recorded every 10 steps in a *NVT* ensemble for 10 ps. The velocity–velocity autocorrelation function from the trajectory of each atom in the MD simulation, whose Fourier transformation gives the DOS,[37,38]

$$g(\omega) = \int e^{i\omega t} \frac{\langle v(t)v(0)\rangle}{\langle v(0)v(0)\rangle} dt, \tag{4}$$

where $v(t)$ is atom velocity at time t, and $v(0)$ is atom velocity of $t = 0$. The DOS of the two crystals was evaluated independently.

The results of phonon DOS for the two crystals in a 15.18° bicrystal are plotted in Fig. 9(a). It is obvious that the phonon DOS has no difference between the two crystals in the bicrystal graphene. This rules out the possibility that the thermal interfacial resistance is caused by phonon spectrum mismatch due to crystallographic misorientation as speculated in the previous section. On the other hand, the local vibrational DOS shown in Fig. 9(b) clearly depicts the difference between atoms located at the grain boundary region and atoms far away from the interface. Therefore, one can conclude that it is the structural defects present at the grain boundary region that lead to the phonon spectral mismatch and thereby the interfacial thermal resistance. To this end, the interfacial thermal resistance can be understood as follows: when phonons interact with a grain boundary consisting of arrays of dislocations, some phonons transmit through the interface while others interact with dislocations and diffuse or revert back to the heat source, resulting in depression in the vibrational DOS of C atoms at the grain boundary interface and thus leading to the interfacial thermal resistance.

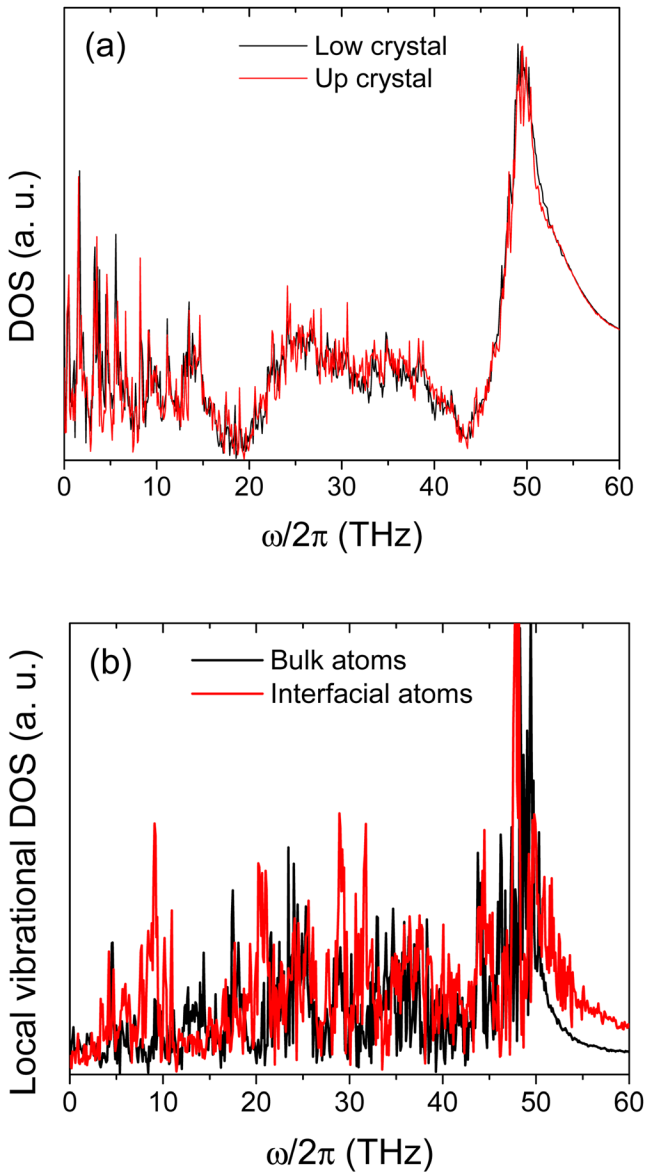

FIG. 9. (Color online) (a) The overall phonon DOS of the two crystals in a 15.18° armchair-oriented bicrystal. The difference between the two curves is indiscernible. (b) The local vibrational DOS of interfacial atoms in comparison with that of bulk atoms, showing the phonon spectral mismatch.

Our recent work on thermal transport behavior in pristine graphene along various directions[31] has shown that thermal transport in graphene is almost isotropic, i.e., no obvious directional preference for heat flux. Based on the above conclusion and the present study results, our MD studies clearly

demonstrate that larger defect density grain boundary gives lower interfacial thermal conductance as shown in Fig. 6(b).

G. Theoretical analysis

To gains some insights on why the thermal conductivity scales inversely with defect density on the grain boundary, we have carried some simple analytical analysis as follows:

The Boltzmann transport equation is generally used to study phonon transport in solids,

$$\frac{\partial N}{\partial t} + v \cdot \nabla N = \left(\frac{\partial N}{\partial t}\right)_{scatter}, \tag{5}$$

where $N(\boldsymbol{r}, \boldsymbol{p}, t)$ is the non-equilibrium phonon distribution, which is a function of time t, particle position vector $\boldsymbol{r}$, momentum vector $\boldsymbol{p}$, and v is the phonon group velocity. The left-hand side of Eq. (5) is the phonon drift term induced by the applied thermal gradient and the right-hand side is the collisional term arising from scattering of the phonons.

In solving Eq. (5), the single-model relaxation time approximation can be used to calculate thermal transport in a variety of systems.[39–41] The single-mode relaxation time approximation assumes that each phonon mode is characterized by a relaxation time that is independent of all other phonons present in the system. With the relaxation time approximation, the scattering term is[42,43]

$$\left(\frac{\partial N}{\partial t}\right)_{scatter} = \frac{N_0 - N}{\tau} = -\frac{n}{\tau}, \tag{6}$$

where τ_D is the relaxation time and n is the deviation from equilibrium. For scattering by particles or defects, the relaxation time is related to the scattering cross sections[44]

$$\tau = \frac{1}{\eta v \sigma}, \quad \text{or} \quad \frac{1}{\tau} = \eta v \sigma, \tag{7}$$

where η and σ are defect density and scattering cross section, respectively. Because the 5–7 dislocation defects are the only defects considered in the present study, it is reasonable to assume σ is a constant for all bicrystal graphenes.

According to the kinetic law, the lattice thermal conductivity is given by[45]

$$\kappa = \frac{1}{3}\int S(\omega) v^2 \tau(\omega) d\omega, \tag{8}$$

where $S(\omega)d\omega$ is the specific heat per unit volume due to the lattice modes of frequency ω, $d\omega$, v is the phonon velocity, and $\tau(\omega)$ is the effective relaxation time. If the phonons are scattered by various interaction processes, each process contributes additively to the relaxation time.[45]

Equation (8) tells that for a given material the thermal conductivity is proportional to the relaxation time, which according to Eq. (7) is inversely proportional to defect density. Therefore, it is expected that the thermal conductivity is a linear function of the reciprocal of defect concentration, which explains our MD results shown in Fig. 7(b).

IV. CONCLUSIONS

In summary, non-equilibrium MD simulations were carried out to study the thermal transport behavior in graphene consists of symmetric tilt grain boundaries. Particular attention was given to the effects of defect density at grain boundaries on the phonon transmission efficiency and the resulting Kaptiza conductance. We found that the Kapitza conductance increases with the conducting length of graphene and saturates at about 200–300 nm, which is the effective ballistic length of graphene. The plausible explanation for such length dependence is that long-wavelength phonons allowable in longer graphene open up new channels for phonons to transmit through the interface. In other words, when the conducting length is shorter than the effective ballistic length of graphene, the scattering between grain boundaries and phonons with wavelength smaller than effective ballistic length will further increase the interfacial thermal resistance. The length independent Kapitza conductance of symmetric grain boundaries we predicted ranges from 19 to 47 GW/Km^2, which is larger than any other thermal electrical interfaces reported in the current literature. Because of the short graphene length used in our simulations ($\sim$400 nm), the overall thermal conductivity of bicrystal graphene we obtained is $\sim$1100 W/mK, which is lower than the experimental value 2000–3000 W/mK.

The Kapitza conductance was found to monotonically increase with temperature, opposite to trend of thermal conductivity in bulk graphene. The Kapitza resistance at the grain boundary of a bicrystal graphene is mainly due to mismatch of phonon spectrum between interfacial atoms and bulk atoms while the bulk resistance in pristine graphene is caused mainly by scattering of phonons, which is enhanced at elevated temperatures. The overall effective thermal conductance of the bicrystal is higher at lower temperatures above room temperature.

It is found that the Kapitza conductance decreases monotonically with increasing GB misorientation angle for both zig-zag and armchair oriented bicrystal graphene. Furthermore, the thermal conductivity scales inversely with dislocation (pair) density for both types of dislocations but with different slops. We also found that the type of dislocations plays a significant role. Specifically, (1, 0) type of dislocations are more efficient in transmitting heat than (1,0) + (0,1) dislocation pair and therefore result in larger interfacial thermal conductance. The vibrational DOS of atoms located at grain boundary regions deviates from that of bulk atoms, suggesting the origin of the interfacial thermal resistance mainly arises from phonon spectral mismatch between local defected atoms and bulk atoms. To this end, the relationship between grain boundaries structure and its effects on thermal properties of graphene has been established.

ACKNOWLEDGMENTS

Computations were performed on the QUEST high performance computing cluster at Northwestern University. The work is supported in part by DARPA through contract N66001-09-C-2012. The views expressed are those of the authors and do not reflect the official policy or position of the Department of Defense or the U.S. Government.

[1]A. A. Balandin, Nature Mater. **10**, 569 (2011).
[2]S. Ghosh, W. Z. Bao, D. L. Nika, S. Subrina, E. P. Pokatilov, C. N. Lau, and A. A. Balandin, Nature Mater. **9**, 555 (2010).
[3]D. L. Nika, S. Ghosh, E. P. Pokatilov, and A. A. Balandin, Appl. Phys. Lett. **94**, 203103 (2009).
[4]K. F. Mak, M. Y. Sfeir, Y. Wu, C. H. Lui, J. A. Misewich, and T. F. Heinz, Phys. Rev. Lett. **101**, 4 (2008).
[5]A. K. Geim and K. S. Novoselov, Nature Mater. **6**, 183 (2007).
[6]A. K. Geim, Science **324**, 1530 (2009).
[7]C. Lee, X. D. Wei, J. W. Kysar, and J. Hone, Science **321**, 385 (2008).
[8]X. B. Yang, G. X. Liu, M. Rostami, A. A. Balandin, and K. Mohanram, IEEE Electron Device Lett. **32**, 1328 (2011).
[9]X. B. Yang, G. X. Liu, A. A. Balandin, and K. Mohanram, ACS Nano **4**, 5532 (2010).
[10]G. Lu, L. E. Ocola, and J. Chen, Appl. Phys. Lett. **94**, 083111 (2009).
[11]A. Cao, Z. Liu, S. Chu, M. Wu, Z. Ye, Z. Cai, Y. Chang, S. Wang, Q. Gong, and Y. Liu, Adv. Mater. **22**, 103 (2010).
[12]J. Wu, H. A. Becerril, Z. Bao, Z. Liu, Y. Chen, and P. Peumans, Appl. Phys. Lett. **92**, 263302 (2008).
[13]A. Cao, J. Qu, M. Yao, and IEEE, in *2010 Proceedings of the 60th Electronic Components and Technology Conference*, pp. 417–420.
[14]Q. K. Yu, J. Lian, S. Siriponglert, H. Li, Y. P. Chen, and S. S. Pei, Appl. Phys. Lett. **93**, 113103 (2008).
[15]K. S. Kim, Y. Zhao, H. Jang, S. Y. Lee, J. M. Kim, J. H. Ahn, P. Kim, J. Y. Choi, and B. H. Hong, Nature **457**, 706 (2009).
[16]X. S. Li, W. W. Cai, J. H. An, S. Kim, J. Nah, D. X. Yang, R. Piner, A. Velamakanni, I. Jung, E. Tutuc, S. K. Banerjee, L. Colombo, and R. S. Ruoff, Science **324**, 1312 (2009).
[17]M. P. Levendorf, C. S. Ruiz-Vargas, S. Garg, and J. Park, Nano Lett. **9**, 4479 (2009).
[18]A. H. Castro Neto, F. Guinea, N. M. R. Peres, K. S. Novoselov, and A. K. Geim, Rev. Mod. Phys. **81**, 109 (2009).
[19]C. Carraro and D. R. Nelson, Phys. Rev. E **48**, 3082 (1993).
[20]A. Bagri, S.-P. Kim, R. S. Ruoff, and V. B. Shenoy, Nano Lett. **11**, 3917 (2011).
[21]O. V. Yazyev and S. G. Louie, Phys. Rev. B **81**, 195420 (2010).
[22]A. A. Balandin, S. Ghosh, W. Z. Bao, I. Calizo, D. Teweldebrhan, F. Miao, and C. N. Lau, Nano Lett. **8**, 902 (2008).
[23]P. Jund and R. Jullien, Phys. Rev. B **59**, 13707 (1999).
[24]S. Plimpton, J. Comput. Phys. **117**, 1 (1995).
[25]L. Lindsay and D. A. Broido, Phys. Rev. B **81**, 205441 (2010).
[26]J. Maultzsch, S. Reich, C. Thomsen, H. Requardt, and P. Ordejon, Phys. Rev. Lett. **92**, 075501 (2004).
[27]M. Mohr, J. Maultzsch, E. Dobardzic, S. Reich, I. Milosevic, M. Damnjanovic, A. Bosak, M. Krisch, and C. Thomsen, Phys. Rev. B **76**, 035439 (2007).
[28]P. L. Kapitza, *Collected Papers of P. L. Kapitza* (Pergamon Press, Oxford, 1967).
[29]V. Samvedi and V. Tomar, Nanotechnology **20**, 365701 (2009).
[30]P. K. Schelling, S. R. Phillpot, and P. Keblinski, J. Appl. Phys. **95**, 6082 (2004).
[31]A. Cao and J. Qu (unpublished).
[32]J. Diao, D. Srivastava, and M. Menon, J. Chem. Phys. **128**, 164708 (2008).
[33]P. E. Pehrsson, W. Zhao, J. W. Baldwin, C. H. Song, J. Liu, S. Kooi, and B. Zheng, J. Phys. Chem. B **107**, 5690 (2003).
[34]E. Pop, D. Mann, Q. Wang, K. Goodson, and H. Dai, Nano Lett. **6**, 96 (2006).
[35]P. Kim, L. Shi, A. Majumdar, and P. L. McEuen, Phys. Rev. Lett. **87**, 215502 (2001).
[36]D. L. Nika, E. P. Pokatilov, A. S. Askerov, and A. A. Balandin, Phys. Rev. B **79**, 12 (2009).
[37]M. T. Dove, *Introduction to Lattice Dynamics* (Cambridge University Press, Cambridge, 1993).
[38]J. R. Lukes and H. Zhong, J. Heat Transfer **129**, 705 (2007).
[39]A. J. H. McGaughey and M. Kaviany, Phys. Rev. B **69**, 094303 (2004).
[40]A. S. Henry and G. Chen, J. Comput. Theor. Nanosci. **5**, 141 (2008).
[41]J. E. Turney, E. S. Landry, A. J. H. McGaughey, and C. H. Amon, Phys. Rev. B **79**, 075316 (2009).
[42]J. M. Ziman, *Electrons and Phonons* (Oxford University Press, Oxford, 1960).
[43]J. Callaway, *Quantum Theory of the Solid State* (Oxford University Press, Oxford, 1991).
[44]W. Kim and A. Majumdar, J. Appl. Phys. **99**, 7 (2006).
[45]P. G. Klemens, Proc. R. Soc. London, Ser. A **208**, 108 (1951).